#### Title:

Arginine Vasopressin-Containing Neurons of the Suprachiasmatic Nucleus Project to CSF

Abbreviated title: SCN vasopressin neurons project to CSF

#### **Authors:**

Alana Taub <sup>1</sup>, Yvette Carbajal <sup>2</sup>, Kania Rimu <sup>2</sup>, Rebecca Holt <sup>2</sup>, Yifan Yao<sup>1</sup>, Amanda L. Hernandez <sup>1</sup>, Joseph LeSauter<sup>2</sup> and Rae Silver <sup>1,3</sup>

- <sup>1</sup>Departments of Psychology, Columbia University, New York, NY, 10027
- <sup>2</sup>Department of Neuroscience, Barnard College, New York, NY 10027.
- <sup>3</sup>Department of Pathology and Cell Biology, Graduate Faculty, Columbia University Medical School, New York, NY 10032.

## **Corresponding Author:**

Rae Silver, Department of Psychology, Mail Code 5501, Columbia University, 1190 Amsterdam Avenue, New York, NY 10027, eMail: Rae.Silver@columbia.edu.

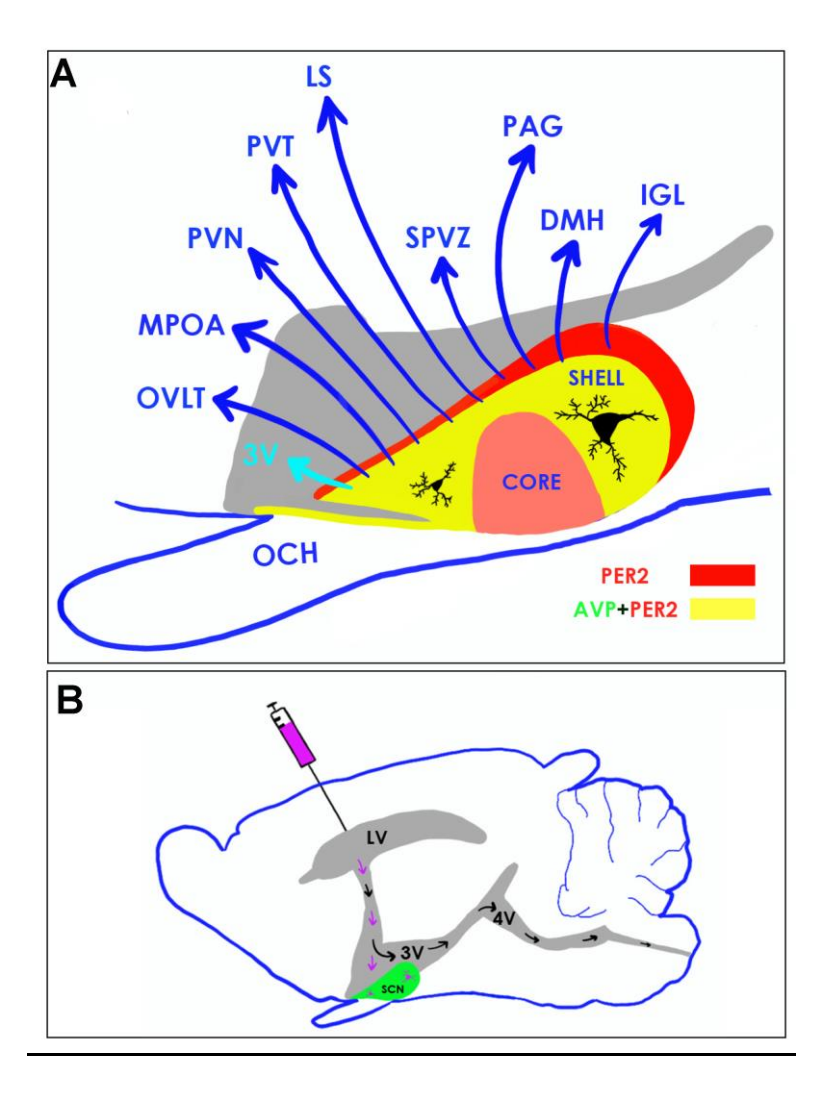
Number of figures: 11 (10 for main manuscript + visual abstract)

Number of tables: 1 Number of words Abstract 242 Introduction 635 Discussion 1070

<u>Acknowledgments:</u> Imaging was performed with support from the <u>the Barnard College Imaging Facility and the National Science Foundation (NSF 1828264).</u>

**Conflicts of Interest**: The authors declare no competing financial interests.

<u>Funding sources</u>: This work was supported by National Science Foundation Grants 1256105 and 1749500 (to R.S.).



**Visual abstract**! While it is well established that there are robust circadian rhythms of arginine vasopressin (AVP) in the cerebrospinal fluid (CSF), the route whereby the peptide reaches the CSF is not clear. (**A**) AVP neurons constitute the largest fraction of the SCN neuronal population. Here we show that processes of AVP-expressing SCN neurons cross the epithelium of the  $3^{rd}$  ventricular wall to reach the CSF (black arrows). Additionally, we report rostro-caudal differences in AVP neuron size and demonstrate that the localization of cells expressing the clock protein PER2 extend beyond the AVP population, thereby indicating that the size of this nucleus is somewhat larger than previously understood. (**B**) Following lateral ventricle (LV) injection of cholera toxin beta subunit (CTβ, magenta) the retrograde tracer is seen in AVP neurons of the SCN, supporting the anatomical evidence that AVP neuronal processes directly contact the CSF.

## **Abstract**

Arginine vasopressin (AVP) expressing neurons form the major population in the brain's circadian clock located in the hypothalamic suprachiasmatic nucleus (SCN). They participate in inter-neuronal coupling and provide an output signal for synchronizing daily rhythms. AVP is present at high concentrations in the CSF and fluctuates on a circadian timescale. While it is assumed that rhythms in CSF AVP are of SCN origin, a route of communication between these compartments has not been delineated. Using immunochemistry and cell filling techniques, we determine the morphology and location of AVP neurons in mouse and delineate their axonal and dendritic processes. Cholera toxin β subunit (CTβ) tracer injected into the lateral ventricle tests whether AVP neurons communicate with CSF. Most importantly, the results indicate that AVP neurons lie in close proximity to the 3<sup>rd</sup> ventricle, and their processes cross the ventricular wall into the CSF. We also report that contrary to widely held assumptions, AVP neurons do not fully delineate the SCN borders as PER2 expression extends beyond the AVP region. AVP neurons form a rostral prong originating in the SCN medial- and ventral-most aspect. AVP is lacking in the mid-dorsal shell but does occur at the base of the SCN just above the optic tract. Finally, neurons of the rostral SCN are smaller than those lying caudally. These findings extend our understanding of AVP signaling potential, demonstrate the heterogeneity of AVP neurons, and highlight limits in using this peptide to delineate the mouse SCN.

# **Significance Statement**

There is a high amplitude circadian rhythm of arginine vasopressin (AVP) in the cerebroventricular fluid (CSF), presumed to be of suprachiasmatic nucleus (SCN) origin. There is however, no known route of communication between these compartments. We demonstrate that in the mouse SCN, processes of AVP neurons course toward the 3rd ventricle and cross the ventricular wall to reach the CSF, thereby enabling vasopressinergic signals to reach many brain regions bearing receptors for this peptide. Also, the SCN extends beyond the borders delineated by AVP neurons and rostral AVP neurons are smaller than caudal populations. The work extends our understanding of AVP signaling potential, the heterogeneity of AVP neurons, and highlights limits in using this peptide to delineate the SCN.

#### Introduction

The suprachiasmatic nucleus (SCN) of the hypothalamus, comprised of ~ 20,000 neurons, functions as a circadian clock, coordinating and synchronizing daily rhythms in numerous bodily functions including metabolism, physiology, behavior, and hormone secretion. These neurons contain a substantial array of peptides (Antle & Silver, 2005), among which the best studied synthesize arginine vasopressin (AVP) (van den Pol & Tsujimoto, 1985; Kalsbeek *et al.*, 2010). AVP-expressing neurons form the major population of neurons in the SCN, and are estimated to constitute 37% of the nucleus

(Moore, 2013). Through most of its rostrocaudal extent, AVP perikarya lie within the shell region (Moore, 2013; Lokshin *et al.*, 2015; Varadarajan *et al.*, 2018). It is widely accepted that AVP neurons delineate the boundaries of the SCN and it is thought that AVP neurons provide the major output signal from the SCN (Cassone *et al.*, 1988; Daikoku *et al.*, 1992; Dai *et al.*, 1997; Abrahamson & Moore, 2001; Ramanathan *et al.*, 2006; Moore, 2013).

#### Efferent connections of the SCN

SCN efferents have been extensively studied (Moore, 2013; Morin, 2013) and more specifically, the efferents of AVP neurons have also been explored (LeSauter & Silver, 1998; Kalsbeek *et al.*, 2010) The medial preoptic area, the periventricular and subparaventricular nucleus, dorsomedial hypothalamus and paraventricular nucleus of the thalamus have been identified as targets of SCN AVP neurons. Output from the SCN influences visceral function (Ueyama *et al.*, 1999), REM sleep (Lee *et al.*, 2009), and timing of the LH surge (Williams *et al.*, 2011). However, the extent to which all of these connections originate from SCN or AVP neurons of other origins is not known.

## **AVP expression in the SCN and CSF is rhythmic**

The transcriptional machinery of the core clockwork directly regulates rhythmic expression of AVP in the SCN shell, but not in other AVP-producing neurons (Jin *et al.*, 1999; Silver *et al.*, 1999). The concentration of AVP in the cerebrospinal fluid (CSF), thought to be of SCN origin, fluctuates daily with a peak in the morning (Schwartz & Reppert, 1985; Söderstein *et al.*, 1985; Jolkkonen *et al.*, 1988; Stark & Daniel, 1989; Kalsbeek *et al.*, 2010). Samples from rat CSF and blood definitively demonstrated circadian rhythms in AVP levels in the cerebrospinal fluid (CSF) but not in the blood (Schwartz *et al.*, 1983). This work established the importance of the SCN in producing circadian rhythms in CSF AVP as SCN lesions abolished rhythmicity and reduced measurable levels of the peptide but left open the possibility that neurons of the SCN may trigger AVP release from some other neural sites. Also unknown was the route whereby AVP of SCN origin might reach the CSF, a question in the present study.

#### The present study

While rhythmicity in CSF AVP levels is well established, the question of how AVP of SCN origin might reach the CSF led to the present study. Much of the work on the SCN has been done in coronal sections and this focus neglects the rostral and caudal-most aspects of the nucleus, both of which are rich in AVP containing neurons (Riddle *et al.*, 2017; Varadarajan *et al.*, 2018). Additionally, in coronal sections it is difficult to visualize the close and extended contact of the SCN with the wall of the 3rd ventricle. Here, we first sought to better understand the full extent of AVP neurons in the mouse SCN. This work pointed to dense AVP fibers projecting toward the CSF, a previously unidentified target. To better characterize their axonal and dendritic processes, we filled AVP neurons with biocytin and characterized their afferent and efferent processes using confocal microscopy. To assess communication of AVP neurons with CSF,

immunocytochemistry was used to label the ventricular wall and the tracer cholera toxin beta subunit (CT $\beta$ ), was injected into the lateral ventricle and SCN AVP cells bearing the tracer were identified.

#### **Methods and Materials**

## **Animals and Housing**

Two strains of mice were used to optimize detection of markers of interest with our multi-label protocols. For detection of PER2, we used adult C57BL/NJ mice (Jackson Laboratory, Bar Harbor, ME); for cell filling with biocytin, laboratory bred 15 day old *Per1*-GFP mice (Kuhlman *et al.*, 2000) were used. Mice were group-housed (4/cage) in translucent propylene cages (48 x 27 x 20 cm) in a colony room with a 12:12 hr light:dark cycle at 21± 2 °C and provided with free access to food and water. All procedures were approved by the Columbia University Animal Care and Use Committee.

## Localization of AVP neurons and efferents

Mice were anesthetized with 100 mg/kg of ketamine and 10 mg/kg of xylazine and perfused transcardially with 50 ml of saline followed by 75 ml of 4% paraformaldehyde. Brains were postfixed overnight at 4°C and then cryoprotected in 20% sucrose in 0.1 M phosphate buffer .9% saline (PBS). For immunochemistry (ICC) sections (50 µm) were cut in the sagittal, horizontal or coronal planes on a cryostat (Microm HM 500M, Walldorf, Germany) and collected into 0.1 M PBS. The brain sections were processed as free-floating sections in 24 well plates. For single label ICC, sections were washed in 0.1M phosphate buffer 0.9% saline (PBS) +0.1 % Triton-X 100 and then blocked with normal donkey serum for 1 hr on a shaker at room temperature. Sections were washed 3 x10 min in PBS and placed in a 0.3%(PBST) solution containing rabbit anti-AVP antibody at 4°C for 48 hrs. Sections were washed (3x) and incubated for 2 hr at RT in .3%PBST containing the appropriate secondary antibody. Sections were washed in PB, mounted, dehydrated in ethanol solutions, cleared in CitriSolve (Fisher Scientific) and coverslipped with Krystalon (EM Diagnostics, Gibbstown, NJ). For double label ICC, the same procedure was used except primary antibodies were either mouse anti-AVP and rabbit anti-PER2; mouse anti-AVP and rabbit anti-S100β or rabbit anti-AVP and goat anti-CT $\beta$ . The appropriate fluorescent secondaries were used (Table 1).

#### AVP in relation to the ependymal wall

To assess AVP fibers in supra and sub-ependymal zones of the 3rd ventricle, we observed AVP and S100 $\beta$  labelled sections (n=5 female mice). S100 $\beta$  stains ependymal cells (Didier *et al.*, 1986; Carlen *et al.*, 2009; Lavado & Oliver, 2011).

## Biocytin filling of patched AVP cells to determine morphology of AVP neurons

To determine the morphology of AVP neurons and their axonal and dendritic projections, *Per1*-GFP mice were sacrificed by cervical dislocation between ZT 12 and 15 (when PER1-GFP expression is high), and cells were patched and filled with biocytin as described for GRP-GFP cells (Drouyer *et al.*, 2010). For immunochemistry of sections bearing biocytin-filled cells tissue was incubated overnight at 4°C with Cy2 streptavidin (Jackson ImmunoResearch, West Grove, PA) in PBST, then processed as above except primary antibodies were guinea pig anti-AVP and rabbit anti-GFP, stained with the appropriate secondary antibodies.

## **Analysis of Biocytin filling**

Each filled cell was examined throughout the z stack using confocal microscopy to assess whether it was single, double or triple labeled for biocytin (green), PER1-GFP (magenta) and AVP (blue). Of 73 cells filled with biocytin in 9 animals, 53 were PER1-GFP positive and 20 were PER1-GFP negative. Of the 53 PER 1-GFP positive cells, 30 were AVP+ and 23 were AVP-. The 20 PER1-GFP negative cells were also AVP negative. Axons originate from the soma or from a proximal dendrite and are very fine and beady. Dendrites are larger and possess spines, swellings and/or appendages [described in (van den Pol, 1980)].

#### Measuring cell size

In the initial study, confocal microscopy was used to measure the perimeter of distinct populations of AVP neurons, enabling comparison with previous studies of this population (Campos *et al.*, 2014, Moore et al., 2002). Images were taken from the rostral- and caudal-most aspects, at the largest extent of the SCN - the mid-region in sagittal sections (2 sections/SCN, n=8 SCNs). The cells were measured at their greatest extent, where a distinct nucleus was seen on the  $1\mu m$  z-axis optical section. The perimeter was determined using the "Annotations and Measurements" tool on NIS-Elements Advance Research software. Seven to 21 cells were measured/region for each brain section (total N= 76 rostral, 89 caudal cells). For volumetric measures, a new set of confocal images of AVP stained SCNs were imported into the imaging software Aivia (Version 9, DRVISION Technologies LLC, Bellevue, WA). The segmentation

output in the pixel classifier tool allows for visualization of the cells in 3D and was used to measure volume of individual rostral (N=88) and caudal (N=101) cells.

#### CTB tracer, lateral ventricle injection site

While CT $\beta$  is an anterograde and retrograde tracer, it behaves primarily as a retrograde tracer at the doses and sites described here (see (Leak & Moore, 2012) for extended discussion and explanation). CalB-GFP mice were anesthetized with 100 mg/kg of ketamine and 10 mg/kg of xylazine at ZT14 and prepared for aseptic surgery. The head was shaved and the mouse was positioned in a stereotaxic apparatus (David Kopf Instruments, Tujanga, CA). Injections were aimed at the lateral ventricle (AP +1.1, ML +0.7 from Bregma, DV –3.0 from the top of the skull). Pressure injections of 4  $\mu$ l of CT $\beta$  (1% low salt solution, List Biologicals, Campbell, CA) were made with a 10  $\mu$ l syringe (Hamilton Co., Reno, NV) at a rate of 2  $\mu$ l per min. The cannula was left in the brain at the end of the infusion for an additional 2 min and removed slowly over 1 min to minimize tracer diffusion upon needle withdrawal. The animals were sacrificed 7 days following surgery. Mice (n=8) were injected with CT $\beta$ . The injection penetrated the lateral septum in 3 brains but was strictly localized to the lateral ventricle in 5 injections (Fig. 1).



**Figure 1**: Lateral ventricle injection sites. Light microscope images of a  $50\mu m$  section showing the injection site for CT $\beta$  in the lateral ventricle. Some CT $\beta$  tracer "en passage" is seen in corpus callosum and cortex, but the SCN does not project to these areas. Injection site in (A) is for SCN shown in Fig. 9, and in (B) for Fig. 10.

## **Microscopy**

Immunofluorescent labeling was examined on a Nikon Eclipse E800 (Morrell Instruments, Melville, NY) microscope using the filters 480±40 nm for Cy2, 560±40 nm for Cy3 and 620±40 nm for Cy5. Images were captured with a USB-3 DMK33UX174

camera (Morrell Instruments) using the Nikon NIS-Elements Basic Research software. To identify AVP dendrites and axons in biocytin-filled cells, and to determine their relation to the CSF, images were taken on a Nikon Eclipse Ti2E confocal microscope (Nikon, Melville, NY) equipped with a LUNV Laser unit and an argon-krypton laser using the excitation wavelengths 488 nm for Cy2, 561 nm for Cy3 and 638 nm for Cy5. NIS Elements Advanced Research software was used to visualize the z-stacks. Confocal images of sections from CT $\beta$ -injected mice were analyzed to determine the colocalization of CT $\beta$  with AVP. The images were imported into Photoshop (Adobe Photoshop CS. Berkeley, CA). Single labelled CT $\beta$  and AVP and double labelled cells were counted by two experimenters (agreement: 93 ± 2%).

## Image analysis

For visualization of cells and/or fibers, we used Photoshop. To recover lost details in dark and bright areas of the image "Shadows" and "Highlights" were adjusted in the "Image-Adjustment-Levels" dialog box in Photoshop, by dragging the black and white "Input Levels" to the edge of the first group of pixels on either end of the histogram (Figs. 4 and 5). The function of "Shadows" and "Highlights" is to brighten areas of shadow and darken areas of brightness based on surrounding pixels; it does not simply lighten or darken an image (Adobe Photoshop CS6). For color images, "Shadows" and "Highlights" were manipulated for each color separately. Grayscale images were inverted prior to these visual optimizations.

<u>Table 1. Primary and secondary antibodies used. \*catalog number as RRID not available.</u>

Antibodies	Host	Dilution	Company	RRID
AVP	Mouse	1:500	Santa Cruz Biotechnology, Santa Cruz, CA	sc-390723 *
AVP	Rabbit	1:5000	Immunostar, Hudson, WI	AB_572219
AVP	Guinea Pig	1:5000	Peninsula Laboratories, San Carlos, CA	AB_2313978
PER2	Rabbit	1:500	EMD Millipore, Temecula, CA	AB_1587380
S100β	Rabbit	1:1	Dako, Carpinteria, CA	AB_1587380
СТВ	Goat	1:500	Lists Biologicals, Campbell, CA	AB 10013220
Cy2	Rabbit	1:200	Jackson Immunoresearch, West Grove, PA	AB_2340612
Cy3	Mouse	1:200	Jackson Immunoresearch, West Grove, PA	AB_2340813
Cy3	Rabbit	1:200	Jackson Immunoresearch, West Grove, PA	AB_2307443
Cy3	Goat	1:200	Jackson Immunoresearch, West Grove, PA	AB_2307351
CY5	Guinea Pig	1:200	Jackson Immunoresearch, West Grove, PA	AB_2340462
Other Products				
Normal donkey serum		1:100	Jackson Immunoresearch, West Grove, PA	AB_2337258

NIS Elements software	Morrell Instruments, Melville, NY	SCR_002776
Photoshop	Adobe Photoshop CS. Berkeley, CA	SCR_014199

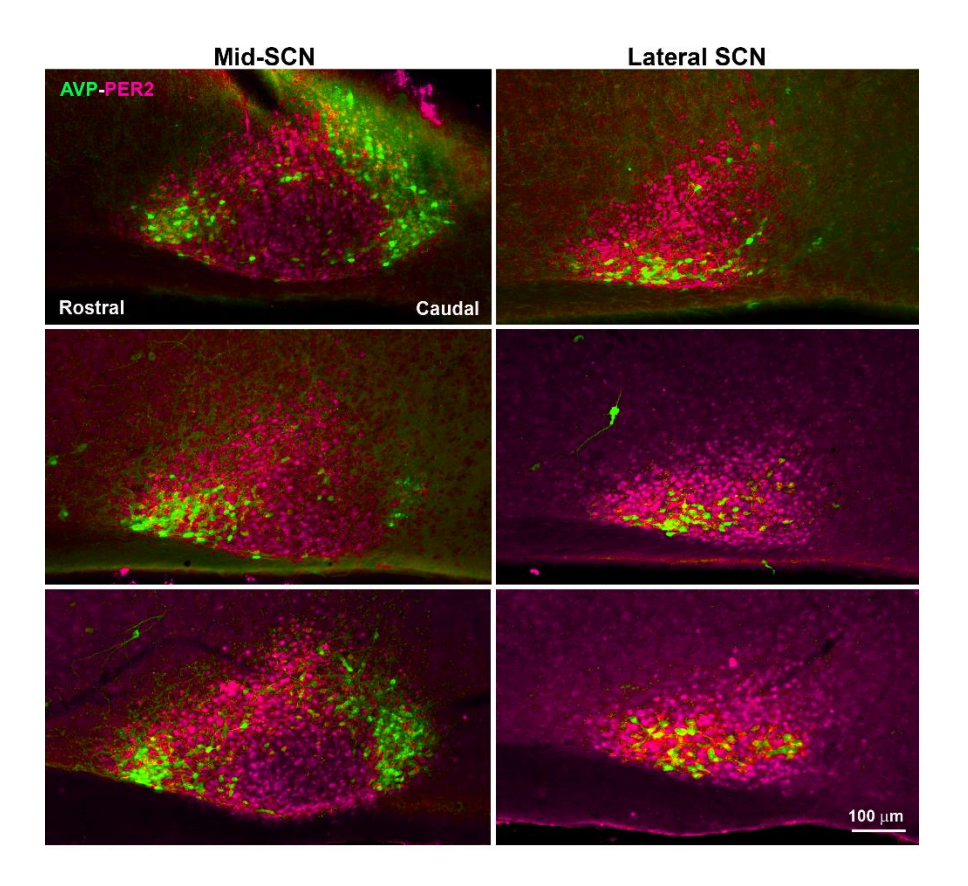
## Statistical analyses:

Data for neuronal perimeter and volume of AVP neurons were measured using both statistical inference and estimation statistics. For statistical inference, we used Student's t-test for normally distributed data with equal variance, Welch's t-test for normally distributed data with unequal variance and Mann-Whitney U test for data lacking normal distribution. For these analyses, outliers were removed (for perimeter, 6 rostral and 4 caudal; for volume, 7 rostral and 2 caudal) using the Tukey method [quartile 1 and 3 ± (1.5\*interguartile range)]. For both perimeter and volume distribution normality was analyzed by the Kolmogorov-Smirnov Test and equality of variances was calculated by F test. For perimeter measures, data for both rostral and caudal are normally distributed (Drostral=0.94, P=0.53; Dcaudal=0.09, p=0.46) but have unequal variance (Srostral=15.21; S<sub>caudal</sub>=35.22, F=0.43, p=0.004). Data grouped within individual SCNs are normally distributed (D<sub>rostral</sub>=0.22, P=0.75; D<sub>caudal</sub>=0.13, p=0.99) and have equal variance (S<sub>rostral</sub>=7.8; S<sub>caudal</sub>=5.9, F=1.31, p=0.73). For volumetric measures, data for all neurons are normally distributed for rostral cells (D<sub>rostral</sub>=0.09, P=0.49), but not for caudal cells (D<sub>caudal</sub>=0.14, p=0.02). The volumetric measures within individual SCN are normally distributed (D<sub>rostral</sub>=0.17, P=0.98; D<sub>caudal</sub>=0.22, p=0.86) and have equal variance (S<sub>rostral</sub>=3432.68; S<sub>caudal</sub>=11576.27, F=0.3, p=0.21)]. Estimation statistics were run using https://www.estimationstats.com/. Mean difference was selected for effect size and 5000 bootstrap samples were run using bias-corrected and accelerated confidence interval (CI) protocols [95% CI lower, upper range] (Ho et al, 2019).

#### Results

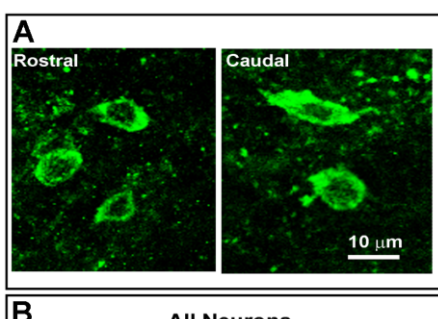
#### **AVP in SCN**

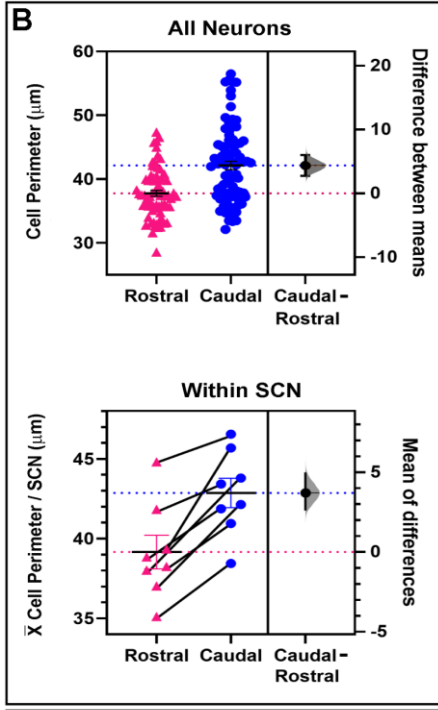
Because AVP-containing neurons are often used to delineate the extent of the SCN, we investigated the accuracy of this protocol by comparing the area of PER2 expression at its peak (ZT12-14) to that of AVP-ir. In sagittal sections, we were surprised to find that at mid and lateral levels of the nucleus, the area of PER2 expression extends well beyond that delineated by AVP (Fig. 2). Most medially PER2 expression corresponds to the area delineated by AVP neurons (not shown).



**Figure 2.** Photomicrographs of sagittal sections at mid-SCN (left) and lateral (right) SCN from 3 representative mice (the most medial aspect is not shown). The results indicate that in mid- and lateral-SCN, PER2 positive neurons extend well beyond the borders of AVP neurons. The mice were euthanized at ZT14 (top two panels) and ZT12 (bottom panel).

As previous studies suggest a relationship between the size of SCN neurons and their location within the nucleus (Campos *et al.*, 2014), we also examined the size of AVP neurons in the rostral versus the caudal SCN measuring both perimeter and volume. The results indicate that neurons lying caudally are larger than rostral ones for both measures and this held true whether statistical inference or estimation statistics were applied (Fig. 3).





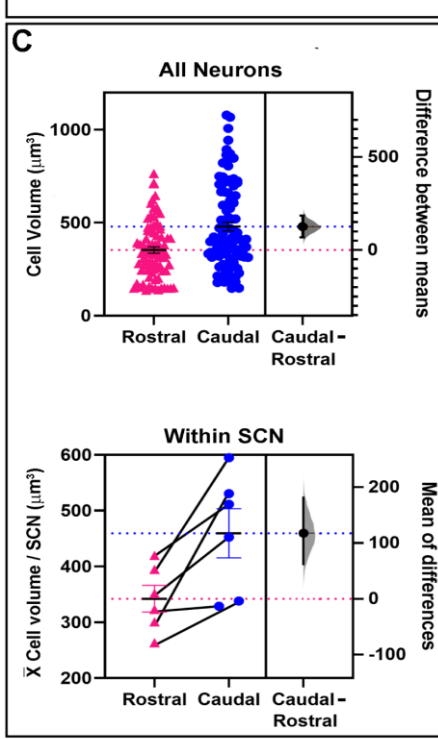


#### Figure 3. Rostral-caudal differences in AVP neurons.

A. Confocal images of representative rostral and caudal cells.

**B**. (Top) Perimeter ( $\bar{X}\pm$  SE) of rostral vs. caudal cells. In all panels, for the estimation statistics the grey curve indicates the entire range of expected sampling error in estimating the mean difference. The horizontal blue and magenta lines are the respective means for the caudal and rostral cells. The mean for rostral cells lies far outside the curve indicating a large difference in size compared to the caudal cells. (Bottom): Perimeter ( $\bar{X}\pm$  SE) of neurons within individual SCNs. The lines connect data for rostral and caudal averages within each SCN.

**C.** (Top) Volume ( $\bar{X}\pm$  SE) of rostral vs. caudal cells. (Bottom) Mean volume ( $\bar{X}\pm$  SE) of neurons within individual SCN. The lines connect data of average volume for rostral and caudal neurons within each SCN.

Measures for perimeter are shown in Fig.(3B). The statistical results are as follows: for cell perimeter (FIG 3B, upper panel), Welch's  $t_{(69,84)} = 5.48$ , p=1.7e-7 [with outliers included, the difference is also significant (Welch's  $t_{(75,88)} = 3.53$ , p=0.0005)]. CI unpaired mean difference is 4.36 [95.0%Cl 2.84, 5.91, p<0.00001. For mean cell perimeter within individual SCNs (FIG 3B, lower panel) Student's paired  $t_{(7)}=5.76$ , \*p=0.0007. Paired mean difference between rostral and caudal is 3.7 [95.0%Cl 2.62, 4.94], p<0.00001. For volume per cell (Fig. 3BC, upper panel),  $z_{(81,89)}=3.65$ , p=0.0003 [with outliers included, the difference is also significant ( $z_{(87,100)}=2.73$ , p=0.006)]. CI unpaired mean difference =1.26x10<sup>2</sup> [95.0%Cl 72.5, 1.84x10<sup>2</sup>], p<0.00001. For mean volume within individual SCNs (Fig. 3C, lower panel), Student's paired  $t_{(5)}=3.44$ , \*p=0.02. Paired mean difference =1.17x10<sup>2</sup> [95.0%Cl 61.2, 1.8x10<sup>2</sup>], p=0.03.

The precise localization of AVP neurons in the main body of the SCN is shown in 7 serial sagittal sections ( $50\mu m$ ) through the extent of the SCN from the medial-most to the lateral-most aspect, in two animals sectioned at slightly different angles. Additionally, a substantial rostral prong is shown in both sagittal and horizontal views (Fig. 4).

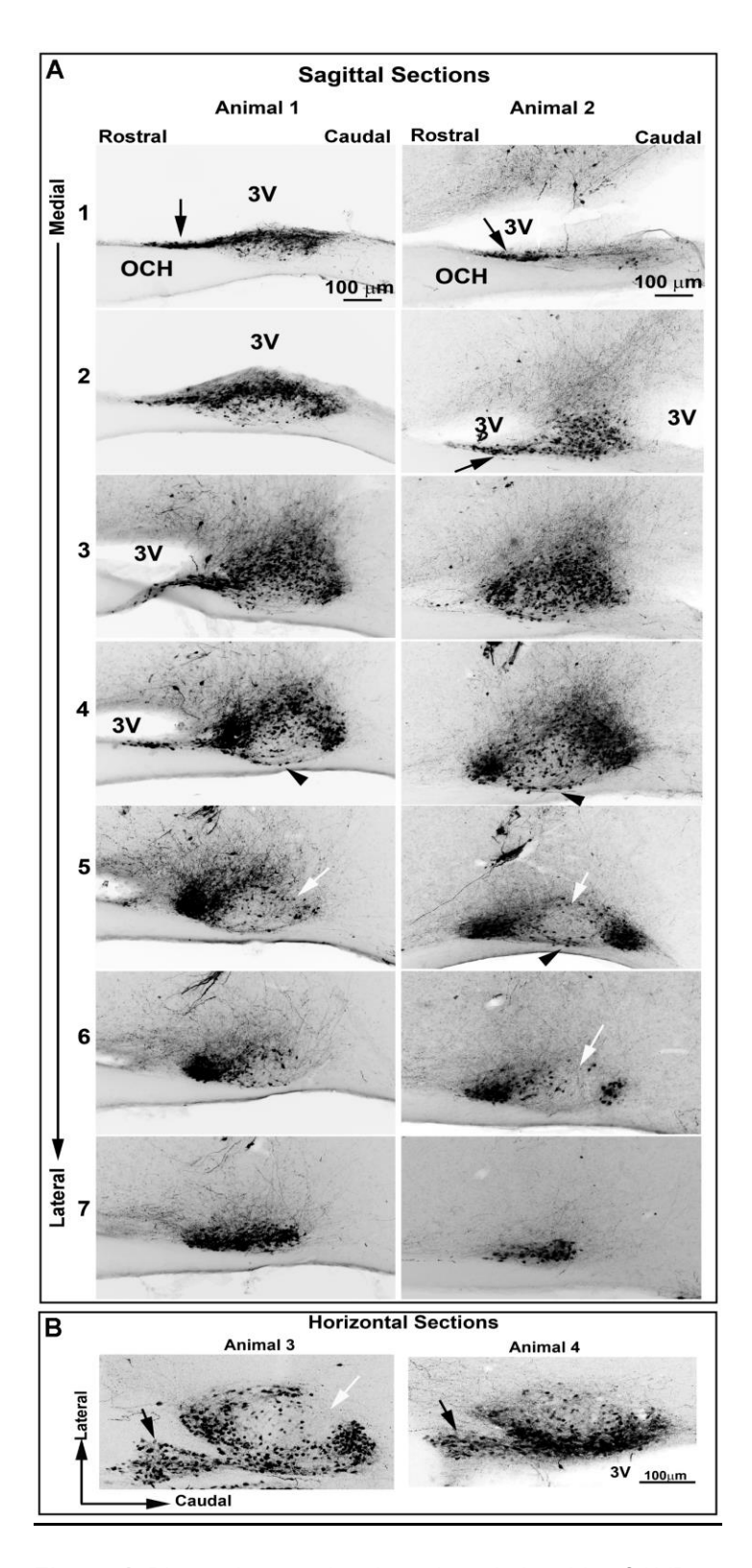


**Figure 4.** Photomicrographs show the relationship of AVP neurons to the CSF in serial sagittal sections from medial to lateral (top images), and in horizontal sections (bottom images). 3V: 3rd ventricle; OCH: optic chiasm.

While the SCN is embedded within the hypothalamus for most of its extent, most medially, it is separated from the rest of the hypothalamus by the 3rd ventricle (Fig. 4, animal #1 and #2, images 1,2). At its dorsal aspect the SCN abuts the 3rd ventricle, most evident when the section is cut perfectly parallel to the midline (Fig. 4, animal #1, images 1 and 2). In animal 1, in sections cut parallel to the midline, the medial SCN is located right below the 3rd ventricle (images 1 and 2). At the mid-level (images 3 to 5), the rostral pole of the SCN abuts the 3rd ventricle and the main body is caudal to the ventricle. Laterally (image 7), the SCN lies entirely within the hypothalamic parenchyma and is no longer in contact with the 3rd ventricle. In animal 2, in sections cut at a different angle, the 3rd ventricle is seen medially (images 1-3), but no longer visible at images 4-7.

At the medial aspect of the SCN, AVP neurons occur throughout the SCN (Fig. 4A, animal #1, image 1; animal #2, images 1 and 2) and these extend in a rostral prong that originates in the ventral part of the nucleus and lies below the  $3^{rd}$  ventricle, just above the optic chiasm (sagittal view Fig. 4A, animal #1, image 1, animal #2, images 1 and 2 and horizontal views Fig. 4B, animals #3 and 4 {black arrows}). The rostral prong extends ~250 um rostrocaudally, 20-30µm dorsoventrally and ~80 µm mediolaterally. At the mid-SCN at its greatest extent in the sagittal view, AVP neurons lie rostrally and caudally, but are sparse in the core and in the mid-dorsal aspect (both animals, images 5; animal #2, image 6 {white arrows}). In addition, AVP neurons are present along the base of the SCN (Fig. 4, both animals, images 4; animal #2, image 5 {arrow heads}). At the lateral aspect, the AVP neurons are densely packed (both animals, image 7).

# Relation of AVP fibers to ependymal wall and CSF in coronal and sagittal sections.

In coronal sections, at its greatest extent, the SCN is rich in AVP neurons (Fig. 5A), and many dendrites and axons course toward the CSF (Fig. 5B). In sagittal sections, projections of AVP neurons travel rostrally toward the 3rd ventricle (Fig. 5C, arrow). Close to the midline, the SCN lies directly above the optic chiasm and its dorsal aspect abuts the 3rd ventricle (Fig. 5D). Here AVP fibers, appear to cross the ependymal wall to reach the CSF in the 3rd ventricle.

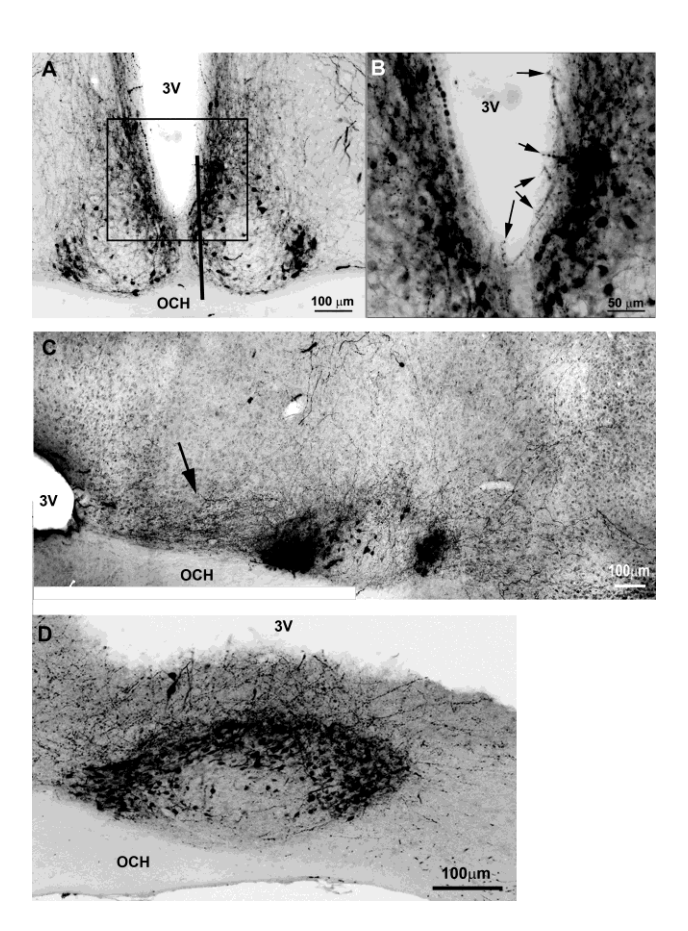


**Figure 5.** Photomicrographs of coronal (A,B) and sagittal (C,D) sections through the SCN show extensive AVP projections coursing toward the CSF. A,B,C are light microscopic images of  $50\mu m$  sections and D is confocal image (z axis:  $2\mu m$ ) **A.** Image of a coronal section of the SCN, stained for AVP showing fibers lying close to CSF. The black box shows the location of the image in B shown at a higher magnification. The black line points to the approximate location of a sagittal section shown in D. **B.** Higher magnification of the SCN shown in A. Arrows point to AVP fibers projecting to the 3rd ventricle. **C.** Sagittal section through mid SCN shows AVP-ir fibers projecting rostrally toward the 3rd ventricle (black arrow). **D.** Confocal image of a sagittal section at the level of the medial SCN [lies at location shown in Fig. 4 (animal #1, image 2)]. Many fibers can be seen coursing towards and possibly crossing the ventricular wall from the SCN to the CSF (z-axis=  $2\mu m$ ). 3V: 3rd ventricle; OCH: optic chiasm.

#### Morphology of axons and dendrites of AVP neurons

To identify the axons and dendrites of AVP neurons, we patched and filled SCN neurons with biocytin. Of the 30 AVP+ neurons studied, 22 had distinguishable axons and dendrites. As previously described (van den Pol, 1980; Abrahamson & Moore, 2001), axonal processes of SCN origin are very thin and exhibit bulbous, irregularly spaced varicosities along their entire length (Fig. 6). Dendrites are larger and possess spines, swellings and/or appendages.

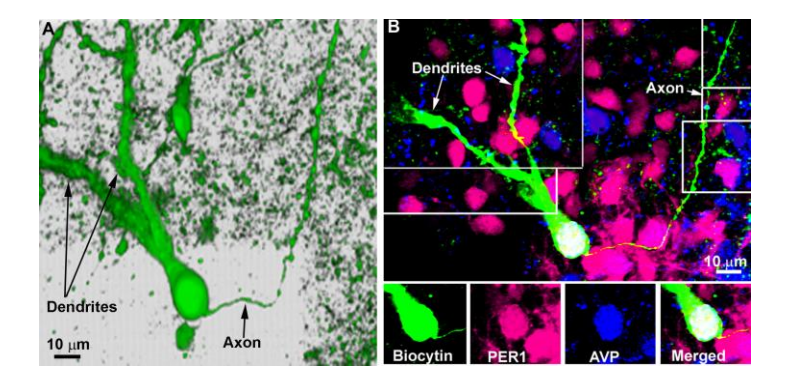


**Figure 6. A**. 3D image of of a biocytin-filled AVP neuron highlighting the distinct morphological features of axons and dendrites. The axon is thin and beady and the dendrites are thicker and bear varicosities and spines.

**B**. Confocal microscopic images showing a montage of the same cell created by aligning 1 mm z-axis images over a z axis of  $18\mu m$ . The bottom row shows the individual peptides within the biocytin-filled cell.

# SCN dendrites and/or axons crossing the ependymal wall

To determine the terminal regions of SCN AVP neurons, we labelled sagittal sections for AVP and S100 $\beta$ , an ependymal wall marker. Some processes appear to terminate subependymaly while others cross into the 3rd ventricle. Both AVP axons (Fig. 7) and dendrites (Fig. 8) extend through the ventricular wall both at the level of the SCN (Fig. 7 A, B, C and Fig. 8 A, C) or near the SCN (Fig. 7 D and 8 B, D). Terminal boutons can be seen within the 3rd ventricle (Fig. 7 B' and C').

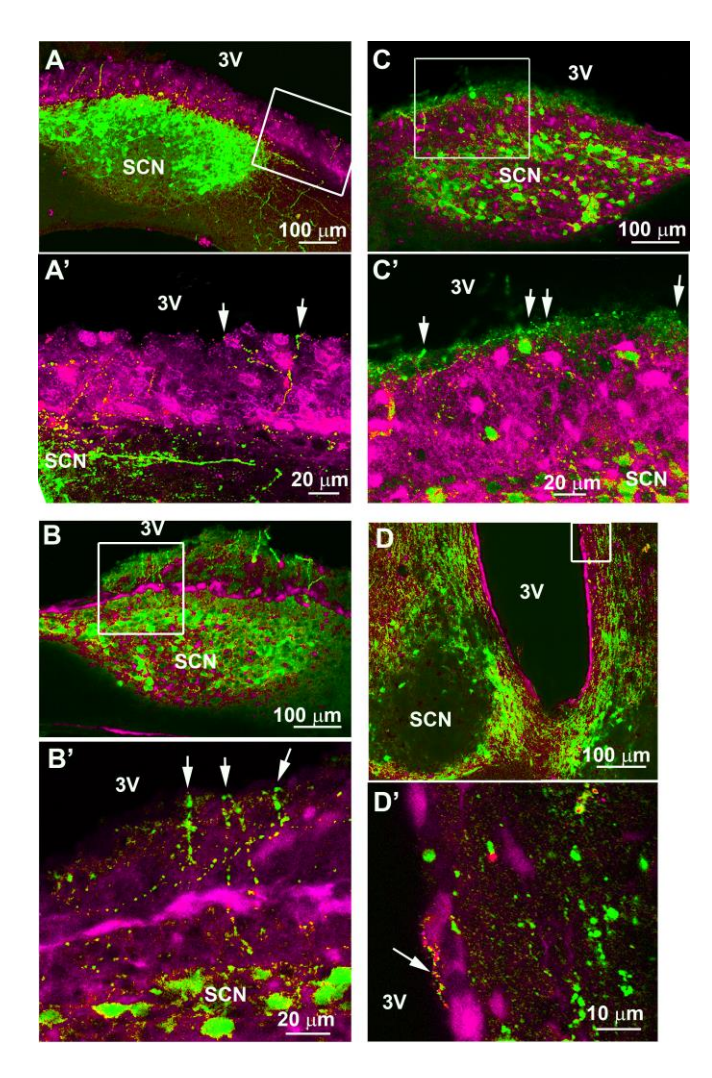


Figure 7. Confocal images of sagittal (**A**, **B**, **C**) and coronal (**D**) sections stained for AVP (green) and S100β (red), a marker of the ependymal wall showing axons at the level of the SCN and nearby, crossing the ventricular wall into the 3rd ventricle. Boxes in **A**, **B**, **C**, **D** show the areas enlarged in **A'**, **B'**, **C'** and **D'**. **A**. Section of the medial SCN (level 2 in Fig. 4) showing many fibers crossing the ventricular wall (z axis: 2.6 μm). **A'**. Image showing the 2 branches of an axon reaching the CSF, caudal to the SCN (arrows; z axis: 1μm). **B** and **C**. Sections (at level 2 in Fig. 4) show AVP fibers extending dorsally from the SCN, crossing the ependymal wall (z axis: B: 2.6 μm, C: 3.5 μm). **B'** and **C'**. Images showing axons crossing the ependymal wall with terminal boutons ending in the 3rd ventricle (arrows; z axis, B' and C': 1.6 microns). **D**. Section showing the SCN and the 3rd ventricle (z axis: 1 μm). D' High magnification images of the area dorsal to the SCN showing an AVP axon coursing on the ventricular side of the ependymal wall (z axis: 0.5 μm). SCN: suprachiasmatic nucleus; 3V: 3rd ventricle.

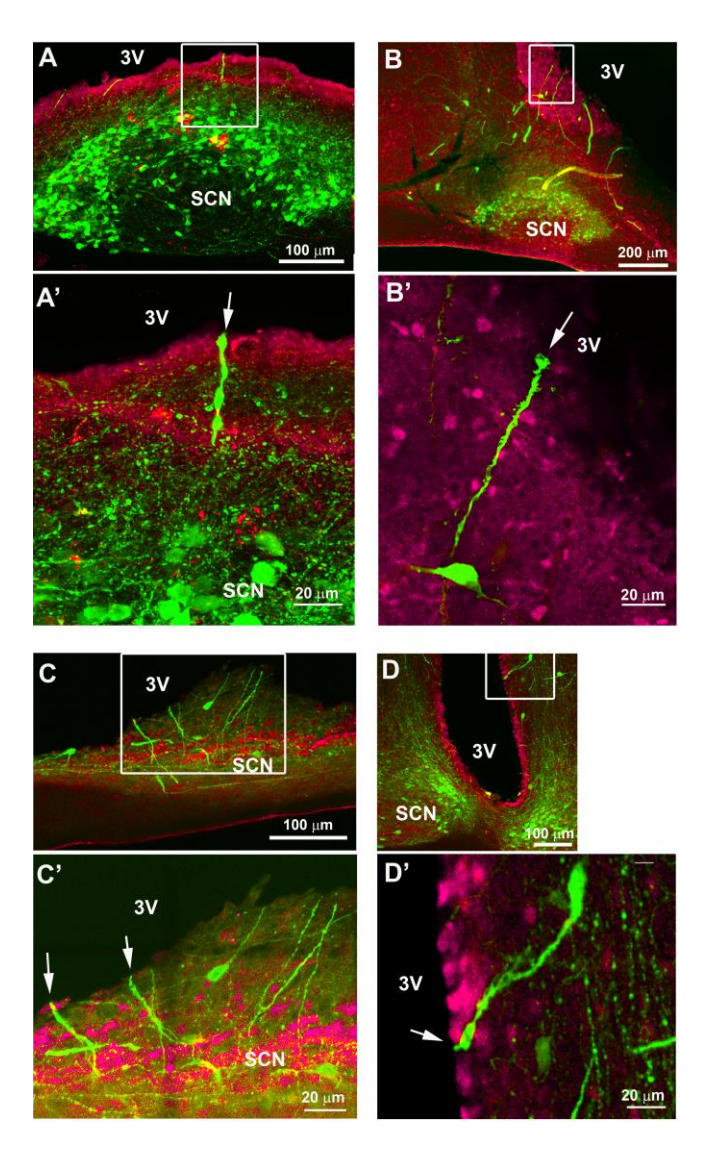


Figure 8. Confocal images of sagittal (A, B, C) and coronal (D) sections stained for AVP (green) and S100β (red), a marker of the ependymal wall showing dendrites at the level of the SCN and nearby, crossing the ventricular wall into the 3rd ventricle. Boxes in A, B, C, D show the areas enlarged in A', B', C' and D'. A. Section of a mid SCN (image 2 in Fig. 4) showing fibers crossing the ventricular wall (z axis: 7 μm). A'. Image showing a large AVP dendrite terminating in the CSF by a bulbous swelling (arrow; z axis: 4 μm). B. AVP dendrites extending toward the 3rd ventricle (z axis: 50 μm). B'. Image showing a dendrite terminating in the 3rd ventricle by a large terminal bulb (arrow; z axis,0.25 μm). C. Sagittal section of a medial SCN (image 1 on Fig. 4) showing fibers extending toward the 3rd ventricle (z axis: 16 μm). C'. Image showing two dendrites terminating in the 3rd ventricle (arrows, z axis:2.5 μm). D. Coronal section showing the SCN and the 3rd ventricle (z axis: 4.3 μm). D'. Image showing a large dendrite, dorsal to the SCN, crossing the ventricular wall, ending in the 3rd ventricle (arrow, z axis: 2.5 μm). SCN: suprachiasmatic nucleus; 3V: 3rd ventricle.

## CTβ tracer in lateral ventricle labels SCN neurons

As noted by (Leak & Moore, 2012), "The CSF contains neuroactive substances that affect brain function and range in size from small molecule transmitters to peptides

and large proteins. CSF-contacting neurons are a well-known and universal feature of non-mammalian vertebrates...". Given the evidence of AVP+ fibers directed to the CSF, we next examined whether AVP cells would uptake the tracer CT $\beta$  from the ventricle. For this, we injected CT $\beta$  into the lateral ventricle. Fig. 9 shows the cells that took up the CT $\beta$  tracer and colocalized with AVP (inset) in the mid SCN. The distribution pattern of CT $\beta$  in the SCN was similar in all 5 animals where injection was restricted to the lateral ventricle.

Of the 4122 AVP and 2488 CT $\beta$  cells evaluated, 15.3 ± 0.9 % AVP were co-labelled with CT $\beta$ . 25.5 ± 1.9 % CT $\beta$  cells were co-labelled with AVP. The results point to extensive input from CSF to SCN neurons bearing AVP.

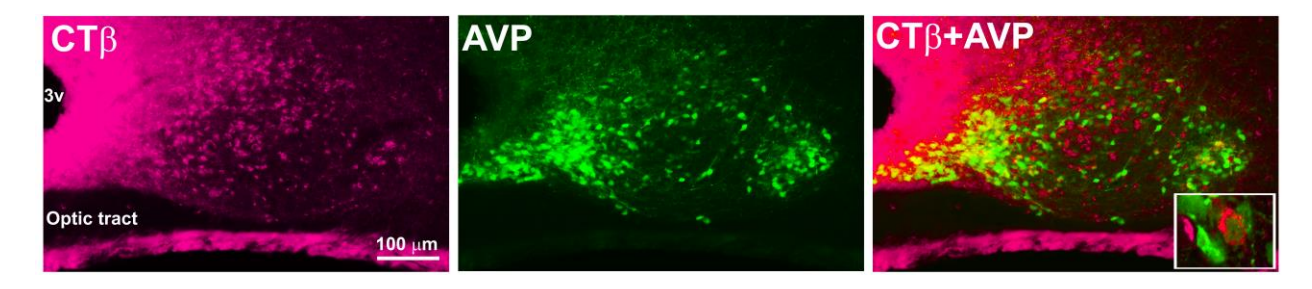


**Figure 9**: Confocal images (z axis: 4  $\mu$ m) of an SCN stained for CT $\beta$  (magenta), AVP (green) and double-labelled. Inset is an image of a cell double labelled for CT $\beta$ +AVP (z axis: 1 micron).

## CTβ in SCN Medial to Lateral

Cells containing  $CT\beta$  are located mostly within the SCN shell where AVP cells are present (Fig. 10). There are a few  $CT\beta$  cells in the very medial SCN (image 1). They are located dorsally in the medial SCN (image 2). In the mid and lateral SCN, they are located mostly within the dorsomedial region and are sparse in the SCN core (images 5-7). They are also numerous in the dorsal area where AVP is sparser (image 5).

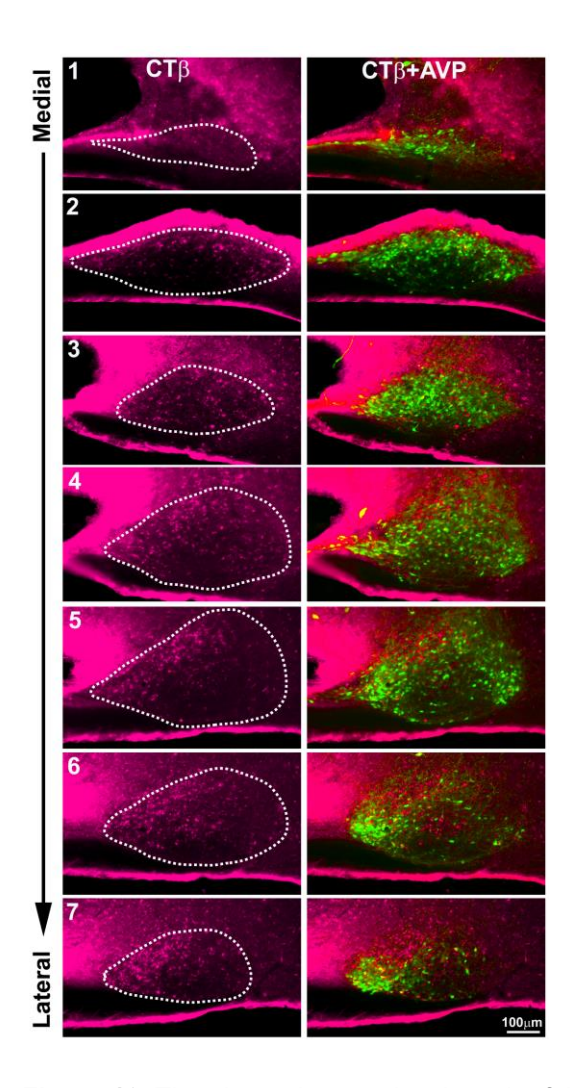


**Figure 10**. The photomicrographs show the full extent of the SCN in sagittal view from its medial to lateral-most aspect in sections labelled for  $CT\beta$  (magenta, left column), and  $CT\beta$ +AVP (right column). The SCN, outlined in white dots, indicates the area used to count cells.  $CT\beta$ =magenta, AVP=green.

#### **Discussion**

#### **AVP fibers reach the CSF**

A major finding of the present study is that SCN AVP neurons course toward and even terminate in the fluid space of the 3rd ventricle. This communication is most obvious in sagittal sections through the SCN, especially near the brain midline. And while AVP neurons have often been used to demarcate the outer borders of the SCN (Vandesande *et al.*, 1975; Sofroniew & Weindl, 1980; Card & Moore, 1984; van den Pol & Tsujimoto, 1985), the sagittal view makes it clear that there are rhythmically expressing PER2 neurons that lie beyond this demarcation, especially at the lateral borders of the nucleus.

Taken together the detailed description of AVP neurons in the SCN make 3 distinct points: AVP cells are at the base of the core region of the SCN (Fig 4). Dorsomedial region of the SCN shell is devoid of AVP neuron, AVP neurons extend rostrally along the midline along a narrow protrusion that originates in the medial-most aspect of the ventral SCN. While each of these details is modest, taken together they can correct incomplete or erroneous anatomical information in previous less detailed work and can provide the groundwork for fine-tuning future studies. Among the questions raised is the nature and function of rhythmic SCN neurons that lie around the outer borders of the SCN and whose existence was not previously realized.

As noted in the introduction, efferent projections of the SCN and more specifically, efferents of AVP neurons of the SCN have been extensively studied (Berk & Finkelstein, 1981; Stephan et al., 1981; Hoorneman & Buijs, 1982; Watts & Swanson, 1987; Watts et al., 1987; Kalsbeek et al., 1993; Morin, 1994; Teclemariam-Mesbah et al., 1999; Leak & Moore, 2001; Moore and Silver, 1998). Although there are some differences among species (Morin, 1994), AVP is a major component of the SCN in most species that have been studied (Morin and Allen 2005). Furthermore, an important contribution of SCN to rhythmic AVP levels in CSF has been known since the mid-1980's, though evidence of the route of communication was lacking. To our knowledge however, there are no prior reports of SCN processes reaching the CSF, though there is light and electron microscopic evidence of (unidentified) somal processes inserted in the ependymal layer or directly contacting the CSF space (Xiao et al., 2005). This may be a consequence of the difficulty of detecting the very fine SCN fibers that course in a rostro-caudal direction (Figs. 4 and 5) especially when they lie right near the midline. The results are consistent with evidence of volume transmission by the SCN and with prior studies. Specifically, paracrine signaling with a role for AVP, has been demonstrated in culture preparations of the SCN (Honma, 2020 [see Fig. 5], Maywood et al., 2011, Tokuda et al., 2018). Furthermore, SCN grafts encapsulated in a polymer material can restore circadian activity rhythms through volume transmission (Silver et al., 1996). Finally, the SCN is densely labeled with CSF injections of more than 20 nl of a tract tracer CTB (Leak & Moore, 2012). More specifically, they showed that within 2 - 10 days of injection, the CTB) label appears in specific groups of neuronal perikarya in the telencephalon, thalamus, hypothalamus and brainstem, many at a considerable distance from the ventricles. They hypothesize that these observations support the view that ventricular CSF is a significant channel for volume transmission and identify those brain regions most likely to be involved in this process.

#### **AVP** neurotransmitters

The role of AVP in rhythmicity has been puzzling in view of the fact that AVP-deficient Brattleboro rats display attenuated but normal circadian rhythms (Groblewski *et al.*, 1981; Brown & Nunez, 1989; Kalsbeek *et al.*, 2010). AVP-containing neurons express GABA and prokineticin 2 (Masumoto *et al.*, 2006; Welsh *et al.*, 2010) pointing to the possibility that these neurons play a broader role in the circadian timing system than

does the AVP protein itself. Mice in which the essential core clock gene *Bmal1* was deleted in AVP neurons (Avp-Bmal1<sup>-/-</sup> mice), had impaired circadian activity rhythms (Mieda *et al.*, 2015) and a gradually expanded interval activity time upon being moved from LD to DD. Bmal1 restoration in AVP neurons of the SCN using a recombinant adeno-associated virus vector reversed the circadian impairment of Avp-Bmal1<sup>-/-</sup> mice. The results were interpreted to mean that the circadian oscillation persists at the cellular level, but that mutual coupling among SCN neurons that regulate activity onset and offset was impaired.

## **Rhythms in SCN-regulated functions**

As noted by van den Pol (van den Pol, 2012) peptide release is difficult to study, as it is seen independent of synaptic specializations, in dendrites, axonal boutons and axon shafts. This is consistent with the possibility that axons and dendrites described here (Fig. 7 and 8) both contribute to the rhythms of AVP in CSF. AVP has a role in the regulation of hydration, blood pressure, body temperature, corticotropin release, and has been implicated in depression, memory, social and sociosexual behavior and in sex differences [reviewed in (de Vries & Miller, 1998; Kalsbeek et al., 2010)]. The stress system in the human brain has been implicated in depression and neurodegeneration (Swaab et al., 2005). The relationship of CSF levels of AVP to plasma levels is of interest in studies of autism, suicide, (Brunner et al., 2002) and personality disorders (Coccaro et al., 1998; Oztan et al., 2018) and the two compartments seem to be separately regulated (Kagerbauer et al., 2013). Much remains to be investigated as understanding the function of this compartment in the context of circadian rhythms requires unravelling a sequence of steps involved in volume transmission. AVP is a phylogenetically ancient molecule of immense versatility with very diverse functions in both the brain and in the periphery (Zelena & Engelmann, 2018). Within the SCN this peptide is important not only as an output signal but also in maintaining synchrony of the SCN network (Shan et al., 2020). A broad view of its potential was suggested decades ago when Gillette and Reppert (Gillette & Reppert, 1987) hypothesized that "Oscillations in AVP secretion and neuronal firing rate potentially represent separate modes by which the SCN transmit time information to other brain regions. The electrical oscillation may relay time-of-day by efferent neuronal output along a limited number of specialized circuits. The AVP secretory rhythm potentially modulates daily rhythm in physiology by a generalized neurohormonal effect." The present work directs attention to the latter possibility.

#### References

ABRAHAMSON, E. E. & MOORE, R. Y. 2001. Suprachiasmatic nucleus in the mouse: retinal innervation, intrinsic organization and efferent projections. *Brain Res*, 916, 172-91.

- ANTLE, M. C. & SILVER, R. 2005. Orchestrating time: arrangements of the brain circadian clock. *Trends Neurosci*, 28, 145-51.
- BERK, M. L. & FINKELSTEIN, J. A. 1981. An autoradiographic determination of the efferent projections of the suprachiasmatic nucleus of the hypothalamus. *Brain Res*, 226, 1-13.
- BROWN, M. H. & NUNEZ, A. A. 1989. Vasopressin-deficient rats show a reduced amplitude of the circadian sleep rhythm. *Physiol Behav*, 46, 759-62.
- BRUNNER, J., KECK, M. E., LANDGRAF, R., UHR, M., NAMENDORF, C. & BRONISCH, T. 2002. Vasopressin in CSF and plasma in depressed suicide attempters: preliminary results. *Eur Neuropsychopharmacol*, 12, 489-94.
- CAMPOS, L. M., CRUZ-RIZZOLO, R. J., WATANABE, I. S., PINATO, L. & NOGUEIRA, M. I. 2014. Efferent projections of the suprachiasmatic nucleus based on the distribution of vasoactive intestinal peptide (VIP) and arginine vasopressin (AVP) immunoreactive fibers in the hypothalamus of Sapajus apella. *J Chem Neuroanat*, 57-58, 42-53.
- CARD, J. P. & MOORE, R. Y. 1984. The suprachiasmatic nucleus of the golden hamster: immunohistochemical analysis of cell and fiber distribution. *Neuroscience*, 13, 415-431.
- CARLEN, M., MELETIS, K., GORITZ, C., DARSALIA, V., EVERGREN, E., TANIGAKI, K., AMENDOLA, M., BARNABE-HEIDER, F., YEUNG, M. S., NALDINI, L., HONJO, T., KOKAIA, Z., SHUPLIAKOV, O., CASSIDY, R. M., LINDVALL, O. & FRISEN, J. 2009. Forebrain ependymal cells are Notch-dependent and generate neuroblasts and astrocytes after stroke. *Nat Neurosci*, 12, 259-67.
- CASSONE, V. M., SPEH, J. C., CARD, J. P. & MOORE, R. Y. 1988. Comparative anatomy of the mammalian hypothalamic suprachiasmatic nucleus. *J. Biol. Rhythms*, 3, 71-91.
- COCCARO, E. F., KAVOUSSI, R. J., HAUGER, R. L., COOPER, T. B. & FERRIS, C. F. 1998. Cerebrospinal fluid vasopressin levels: correlates with aggression and serotonin function in personality-disordered subjects. *Arch Gen Psychiatry*, 55, 708-14.
- DAI, J., SWAAB, D. F. & BUIJS, R. M. 1997. Distribution of vasopressin and vasoactive intestinal polypeptide (VIP) fibers in the human hypothalamus with special emphasis on suprachiasmatic nucleus efferent projections. *J Comp Neurol*, 383, 397-414.
- DAIKOKU, S., HISANO, S. & KAGOTANI, Y. 1992. Neuronal associations in the rat suprachiasmatic nucleus demonstrated by immunoelectron microscopy. *J. Comp. Neurol.*, 325, 559-571.
- DE VRIES, G. J. & MILLER, M. A. 1998. Anatomy and function of extrahypothalamic vasopressin systems in the brain. *Prog Brain Res*, 119, 3-20.
- DIDIER, M., HARANDI, M., AGUERA, M., BANCEL, B., TARDY, M., FAGES, C., CALAS, A., STAGAARD, M., MOLLGARD, K. & BELIN, M. F. 1986. Differential immunocytochemical staining for glial fibrillary acidic (GFA) protein, S-100 protein and glutamine synthetase in

- the rat subcommissural organ, nonspecialized ventricular ependyma and adjacent neuropil. *Cell Tissue Res*, 245, 343-51.
- DROUYER, E., LESAUTER, J., HERNANDEZ, A. L. & SILVER, R. 2010. Specializations of gastrin-releasing peptide cells of the mouse suprachiasmatic nucleus. *J Comp Neurol*, 518, 1249-63.
- GILLETTE, M. U. & REPPERT, S. M. 1987. The hypothalamic suprachiasmatic nuclei: circadian patterns of vasopressin secretion and neuronal activity *in vitro*. *Brain Res. Bull.*, 19, 135-139.
- GROBLEWSKI, T. A., NUNEZ, A. A. & GOLD, R. M. 1981. Circadian rhythms in vasopressin deficient rats. *Brain Res. Bull.*, 6, 125-130.
- HO, L. H., RUFFIN, R. E., MURGIA, C., LI, L., KRILIS, S. A., & ZALEWSKI, P. D. 2004. Labile zinc and zinc transporter ZnT4 in mast cell granules: Role in regulation of caspase activation and NF-κB translocation. *J. Immunol.*, **172**, 7750–7760.
- HONMA, S. 2020. Development of the circadian clock. Eur. J. Neurosci., 51, 182-193.
- HOORNEMAN, E. M. D. & BUIJS, R. M. 1982. Vasopressin fiber pathways in the rat brain following suprachiasmatic nucleus lesioning. *Brain Res.*, 243, 235-241.
- JIN, X., SHEARMAN, L. P., WEAVER, D. R., ZYLKA, M. J., DE VRIES, G. J. & REPPERT, S. M. 1999. A molecular mechanism regulating rhythmic output from the suprachiasmatic nucleus. *Cell*, 96, 57-68.
- JOLKKONEN, J., TUOMISTO, L., VAN WIMERSMA GREIDANUS, T. B. & RIEKKINEN, P. J. 1988. Vasopressin levels in the cerebrospinal fluid of rats with lesions of the paraventricular and suprachiasmatic nuclei. *Neurosci. Lett.*, 86, 184-188.
- KAGERBAUER, S. M., MARTIN, J., SCHUSTER, T., BLOBNER, M., KOCHS, E. F. & LANDGRAF, R. 2013. Plasma oxytocin and vasopressin do not predict neuropeptide concentrations in human cerebrospinal fluid. *J Neuroendocrinol*, 25, 668-73.
- KALSBEEK, A., FLIERS, E., HOFMAN, M. A., SWAAB, D. F. & BUIJS, R. M. 2010. Vasopressin and the output of the hypothalamic biological clock. *J Neuroendocrinol*, 22, 362-72.
- KALSBEEK, A., TECLEMARIAM-MESBAH, R. & PÉVET, P. 1993. Efferent projections of the suprachiasmatic nucleus in the golden hamster (mesocricetus auratus). *J. Comp. Neurol.*, 332, 293-314.
- KUHLMAN, S. J., QUINTERO, J. E. & MCMAHON, D. G. 2000. GFP fluorescence reports Periodl circadian gene regulation in the mammalian biological clock. *NeuroReport*, 11, 1479-1482.
- LAVADO, A. & OLIVER, G. 2011. Six3 is required for ependymal cell maturation. *Development*, 138, 5291-300.

- LEAK, R. K. & MOORE, R. Y. 2001. Topographic organization of suprachiasmatic nucleus projection neurons. *J Comp Neurol*, 433, 312-34.
- LEAK, R. K. & MOORE, R. Y. 2012. Innervation of ventricular and periventricular brain compartments. *Brain Res*, 1463, 51-62.
- LEE, M. L., SWANSON, B. E. & DE LA IGLESIA, H. O. 2009. Circadian timing of REM sleep is coupled to an oscillator within the dorsomedial suprachiasmatic nucleus. *Curr Biol*, 19, 848-52.
- LESAUTER, J. & SILVER, R. 1998. Output signals of the SCN. Chronobiol Int, 15, 535-50.
- LOKSHIN, M., LESAUTER, J. & SILVER, R. 2015. Selective Distribution of Retinal Input to Mouse SCN Revealed in Analysis of Sagittal Sections. *J Biol Rhythms*, 30, 251-7.
- MASUMOTO, K. H., NAGANO, M., TAKASHIMA, N., HAYASAKA, N., HIYAMA, H., MATSUMOTO, S., INOUYE, S. T. & SHIGEYOSHI, Y. 2006. Distinct localization of prokineticin 2 and prokineticin receptor 2 mRNAs in the rat suprachiasmatic nucleus. *Eur J Neurosci*, 23, 2959-70.
- MAYWOOD, E. S., CHESHAM, J. E., O'BRIEN, J. A. & HASTINGS, M. H. 2011. A diversity of paracrine signals sustains molecular circadian cycling in suprachiasmatic nucleus circuits. *Proc Natl Acad Sci U S A*, 108, 14306-11.
- MIEDA, M., ONO, D., HASEGAWA, E., OKAMOTO, H., HONMA, K., HONMA, S. & SAKURAI, T. 2015. Cellular clocks in AVP neurons of the SCN are critical for interneuronal coupling regulating circadian behavior rhythm. *Neuron*, 85, 1103-16.
- MOORE, R. Y. 2013. The suprachiasmatic nucleus and the circadian timing system. *Prog Mol Biol Transl Sci*, 119, 1-28.
- MOORE, R. Y. & SILVER, R. 1998. Suprachiasmatic nucleus organization. *Chronobiol Int*, 15, 475-87.
- MOORE, R. Y., SPEH, J. C. & LEAK, R. K. 2002. Suprachiasmatic nucleus organization. *Cell Tissue Res*, 309, 89-98.
- MORIN, L. P. 1994. The circadian visual system. Brain Res. Rev., 67, 102-127.
- MORIN, L. P. 2013. Neuroanatomy of the extended circadian rhythm system. *Exp Neurol*, 243, 4-20.
- MORIN, L. P. & ALLEN, C. N. 2006. The circadian visual system, 2005. *Brain Res Brain Res Rev*.

- OZTAN, O., GARNER, J. P., PARTAP, S., SHERR, E. H., HARDAN, A. Y., FARMER, C., THURM, A., SWEDO, S. E. & PARKER, K. J. 2018. Cerebrospinal fluid vasopressin and symptom severity in children with autism. *Ann Neurol*, 84, 611-615.
- RAMANATHAN, C., NUNEZ, A. A., MARTINEZ, G. S., SCHWARTZ, M. D. & SMALE, L. 2006. Temporal and spatial distribution of immunoreactive PER1 and PER2 proteins in the suprachiasmatic nucleus and peri-suprachiasmatic region of the diurnal grass rat (Arvicanthis niloticus). *Brain Res*, 1073-1074, 348-58.
- RIDDLE, M., MEZIAS, E., FOLEY, D., LESAUTER, J. & SILVER, R. 2017. Differential localization of PER1 and PER2 in the brain master circadian clock. *Eur J Neurosci*, 45, 1357-1367.
- SCHWARTZ, W. J., COLEMAN, R. J. & REPPERT, S. M. 1983. A daily vasopressin rhythm in rat cerebrospinal fluid. *Brain Res.*, 263, 105-112.
- SCHWARTZ, W. J. & REPPERT, S. M. 1985. Neural regulation of the circadian vasopressin rhythm in cerebrospinal fluid: a pre-eminent role for the suprachiasmatic nuclei. *J. Neurosci.*, 5, 2771-2778.
- SHAN, Y., ABEL, J. H., LI, Y., IZUMO, M., COX, K. H., JEONG, B., YOO, S. H., OLSON, D. P., DOYLE, F. J., 3RD & TAKAHASHI, J. S. 2020. Dual-Color Single-Cell Imaging of the Suprachiasmatic Nucleus Reveals a Circadian Role in Network Synchrony. *Neuron*.
- SILVER, R., LESAUTER, J., TRESCO, P. A. & LEHMAN, M. N. 1996. A diffusible coupling signal from the transplanted suprachiasmatic nucleus controlling circadian locomotor rhythms. *Nature*, 382, 810-813.
- SILVER, R., SOOKHOO, A. I., LESAUTER, J., STEVENS, P., JANSEN, H. T. & LEHMAN, M. N. 1999. Multiple regulatory elements result in regional specificity in circadian rhythms of neuropeptide expression in mouse SCN. *NeuroReport*, 10, 3165-3174.
- SÖDERSTEIN, P., DEVRIES, G. J., BUIJS, R. M. & MELIN, P. 1985. A daily rhythm in behavioral vasopressin sensitivity and brain vasopressin concentrations. *Neurosci. Lett.*, 58, 37-41.
- SOFRONIEW, M. V. & WEINDL, A. 1980. Identification of parvocellular vasopressin and neurophysin neurons of the suprachiasmatic nucleus of a variety of mammals including primates. *J. Comp. Neurol.*, 193, 659-675.
- STARK, R. I. & DANIEL, S. S. 1989. Circadian rhythm of vasopressin levels in cerebrospinal fluid of the fetus: effect of continuous light. *Endocrinology*, 124, 3095-101.
- STEPHAN, F. K., BERKLEY, K. J. & MOSS, R. L. 1981. Efferent connections of the rat suprachiasmatic nucleus. *Neuroscience*, 6, 2625-2641.
- SWAAB, D. F., BAO, A. M. & LUCASSEN, P. J. 2005. The stress system in the human brain in depression and neurodegeneration. *Ageing Res Rev, 4*, 141-94.

- TECLEMARIAM-MESBAH, R., TER HORST, G. J., POSTEMA, F., WORTEL, J. & BUIJS, R. M. 1999. Anatomical demonstration of the suprachiasmatic nucleus-pineal pathway. *J Comp Neurol*, 406, 171-82.
- TOKUDA, I. T., ONO, D., HONMA, S., HONMA, K. I. & HERZEL, H. 2018. Coherency of circadian rhythms in the SCN is governed by the interplay of two coupling factors. *PLoS Comput Biol.* 14, e1006607.
- UEYAMA, T., KROUT, K. E., NGUYEN, X. V., KARPITSKIY, V., KOLLERT, A., METTENLEITER, T. C. & LOEWY, A. D. 1999. Suprachiasmatic nucleus: a central autonomic clock. *Nat Neurosci*, 2, 1051-3.
- VAN DEN POL, A. N. 1980. The hypothalamic suprachiasmatic nucleus of rat: intrinsic anatomy. *J. Comp. Neurol.*, 191, 661-702.
- VAN DEN POL, A. N. 2012. Neuropeptide transmission in brain circuits. Neuron, 76, 98-115.
- VAN DEN POL, A. N. & TSUJIMOTO, K. L. 1985. Neurotransmitters of the hypothalamic suprachiasmatic nucleus: immunocytochemical analysis of 25 neuronal antigens. *Neuroscience*, 15, 1049-86.
- VANDESANDE, F., DIERICKX, K. & DEMEY, J. 1975. Identification of the vasopressinneurophysin producing neurons of the rat suprachiasmatic nuclei. *Cell Tissue Res*, 156, 377-80.
- VARADARAJAN, S., TAJIRI, M., JAIN, R., HOLT, R., AHMED, Q., LESAUTER, J. & SILVER, R. 2018. Connectome of the Suprachiasmatic Nucleus: New Evidence of the Core-Shell Relationship. *eNeuro*, 5.
- WATTS, A. G. & SWANSON, L. W. 1987. Efferent projections of the suprachiasmatic nucleus: II. Studies using retrograde transport of fluorescent dyes and simultaneous peptide immunohistochemistry in the rat. *J. Comp. Neurol.*, 258, 230-252.
- WATTS, A. G., SWANSON, L. W. & SANCHEZ-WATTS, G. 1987. Efferent projections of the suprachiasmatic nucleus: I. Studies using anterograde transport of *Phaseolus vulgaris* leucoagglutinin in the rat. *J. Comp. Neurol.*, 258, 204-229.
- WELSH, D. K., TAKAHASHI, J. S. & KAY, S. A. 2010. Suprachiasmatic nucleus: cell autonomy and network properties. *Annu Rev Physiol*, 72, 551-77.
- WILLIAMS, W. P., 3RD, JARJISIAN, S. G., MIKKELSEN, J. D. & KRIEGSFELD, L. J. 2011. Circadian control of kisspeptin and a gated GnRH response mediate the preovulatory luteinizing hormone surge. *Endocrinology*, 152, 595-606.
- XIAO, M., DING, J., WU, L., HAN, Q., WANG, H., ZUO, G. & HU, G. 2005. The distribution of neural nitric oxide synthase-positive cerebrospinal fluid-contacting neurons in the third ventricular wall of male rats and coexistence with vasopressin or oxytocin. *Brain Res*, 1038, 150-62.

ZELENA, D. & ENGELMANN, M. 2018. The Brattleboro Rat: The First and Still Up-to-Date Mutant Rodent Model for Neuroendocrine Research *In:* LUDWIG, M. & LEVKOWITZ, G. (eds.) *Model animals in neuroendocrinology : from worm to mouse to man.* First edition. ed. Hoboken, NJ: Wiley.